Neurocomputing 154 (2015) 174–188

Contents lists available at ScienceDirect

Neurocomputing

journal homepage: www.elsevier.com/locate/neucom

# A real-time topography of maximum contact pressure distribution at medial tibiofemoral knee implant during gait: Application to knee rehabilitation

Marzieh M. Ardestani [a,*], Mehran Moazen [b], Zhenxian Chen [a], Jing Zhang [a], Zhongmin Jin [a,c]

[a] State Key Laboratory for Manufacturing System Engineering, School of Mechanical Engineering, Xi'an Jiaotong University, 710049 Xi'an, Shaanxi, China
[b] Medical and Biological Engineering, School of Engineering, University of Hull, Hull, HU6 7RX, UK
[c] Institute of Medical and Biological Engineering, School of Mechanical Engineering, University of Leeds, Leeds, LS2 9JT, UK

ARTICLE INFO

*Article history:*
Received 19 March 2014
Received in revised form
29 September 2014
Accepted 2 December 2014
Communicated by Bo Shen
Available online 15 December 2014

*Keywords:*
Gait analysis
Rehabilitation
Knee implant
Medial thrust
Trunk sway
Time delay neural network

ABSTRACT

Knee contact pressure is a crucial factor in the knee rehabilitation programs. Although contact pressure can be estimated using finite element analysis, this approach is generally time-consuming and does not satisfy the real-time requirements of a clinical set-up. Therefore, a real-time surrogate method to estimate the contact pressure would be advantageous.

This study implemented a novel computational framework using wavelet time delay neural network (WTDNN) to provide a real-time estimation of contact pressure at the medial tibiofemoral interface of a knee implant. For a number of experimental gait trials, joint kinematics/kinetics and the resultant contact pressure were computed through multi-body dynamic and explicit finite element analyses to establish a training database for the proposed WTDNN. The trained network was then tested by predicting the maximum contact pressure at the medial tibiofemoral knee implant for two different knee rehabilitation patterns; "*medial thrust*" and "*trunk sway*". WTDNN predictions were compared against the calculations from an explicit finite element analysis (gold standard).

Results showed that the proposed WTDNN could accurately calculate the maximum contact pressure at the medial tibiofemoral knee implant for *medial thrust* ($\overline{RMSE}=1.7$ MPa, $\overline{NRMSE}=6.2\%$ and $\overline{\rho}=0.98$) and *trunk sway* ($\overline{RMSE}=2.6$ MPa, $\overline{NRMSE}=9.3\%$, $\overline{\rho}=0.96$) much faster than the finite element method. The proposed methodology could therefore serve as a cost-effective surrogate model to provide real-time evaluation of the gait retraining programs in terms of the resultant maximum contact pressures.



## 1. Introduction

Growing prevalence of knee osteoarthritis (OA) as the main cause of knee arthroplasty on one hand and cost, risk and complications of the surgery on the other hand have led to the significant development of non-surgical gait modifications [1–7]. Gait modification aims to alter walking patterns to decrease knee joint loading through minor changes in gait kinematics. Similarly the load reduction on the artificial knee joint can also be achieved through gait modifications and rehabilitation strategies to minimize wear and prolong the clinical life time of the prosthesis. A number of gait modifications have been reported in the literature to reduce knee joint loading [8–12]. These modification strategies have been mainly designed to offload the knee joint. However, offloading gait interventions may reduce knee contact area, leading to an adverse increase in contact pressure on the joint bearing surfaces. Therefore an off-loading strategy may not be very beneficial and can even be detrimental to the knee joint [13]. Therefore the resultant contact pressure on the articulating surfaces should be considered in clinical implementation of rehabilitation programs.

Finite element analysis (FEA) is a powerful computational technique to calculate contact pressure [14–17]. However this approach is highly time-demanding and computationally expensive. Therefore, FEA is mainly used as a *post-processing* stage for multi-body dynamic analysis to provide tissue-level information. In fact, the available FEA methods do not satisfy the necessity of real-time calculation in a clinical setup. In clinical rehabilitation, patients should be trained to internalize the rehabilitation strategy as their daily walking patterns. Therefore, real-time evaluation of contact pressure benefits the clinical implementation of rehabilitation programs, for example to investigate the effect of a rehabilitation strategy on the knee joint contact pressure.

* Corresponding author. Tel.: +86 29 83395122.
*E-mail address:* mostafavizadeh@yahoo.com (M.M. Ardestani).

http://dx.doi.org/10.1016/j.neucom.2014.12.005
0925-2312/

Artificial intelligence is a relatively new method that has been used in various fields of biomechanics as a real-time surrogate model [18–21]. An artificial intelligent network consists of a number of processor units (neurons) that are densely connected to each other via numeric weights. Once a set of inputs and resultant outputs are presented to the network; the causal relationships between inputs and outputs would be captured and stored in numeric weights. Thus, the network "learns" the interaction between inputs and outputs. Given a "new" set of inputs that has not seen by the network before, the trained neural network (surrogate model) can generalize the relationship to produce the associated output and release the necessity of running the original model and repetition of time consuming calculations [22]. In particular, neural networks have been jointly used with finite element simulation in a variety of biomechanics studies such as load estimation [23–25] and bone remodeling [26,27]. Study of Lu et al. to best of our knowledge is the only study that has used the aforementioned approach to predict the contact pressure [28]. Lu et al. predicted the spatial distribution of contact stress at medial tibia cartilage for a simplified contact model with 400 structural elements. A one-by-one mapping was developed from the three dimensional force data space into the resultant contact stress through a time delay neural network (TDNN). However, their proposed TDNN had a fairly large structure (1200 inputs, 400 outputs and 280 hidden neurons) for a simplified contact model which limits its practical function in realistic application. In fact due to the one-by-one mapping set-up, the proposed TDNN structure cannot be used for a more realistic contact model since increasing the number of elements in the model would increase the number of inputs and outputs resulting in a more complicated structure which requires further number of training data sets. On the other hand, in clinical applications, resultant *maximum contact pressures* are mainly of interests. In this case, the time history of spatial contact pressure distribution is not required. Instead, the maximum contact pressures and the corresponding contact regions that occur over the entire gait cycle should be focused.

The aims of this study were to (1) propose a novel computational framework to predict the distribution of "maximum" contact pressure instead of "spatial" distribution through a simple cost-efficient neural network structure for a realistic contact model, and (2) demonstrate the advantages of the proposed approach in an application to provide a real-time evaluation of knee rehabilitation strategies in terms of maximum contact pressure and corresponding contact regions at the medial tibiofemoral knee implant.

## 2. Materials and methods

Artificial intelligent surrogates require a primary database to describe the "causal" interactions between inputs and outputs [29]. Therefore, a number of gait trials, obtained from literature, were imported to multi-body dynamic (MBD) analysis to estimate knee joint kinematics and kinetics. Resultant kinematics and forces, from MBD analysis, were then used as boundary conditions and load profiles in finite element analysis (FEA) to calculate the contact pressure distribution. A data matrix constructed from knee kinematics/kinetics (inputs) and contact pressures (outputs) served as the required training database for the proposed surrogate model. The overall ability of this surrogate was then tested by predicting the contact pressure for a number of rehabilitation gait trials. It should be pointed out that FEA was used for a twofold purpose: first, to construct the training database and second, as a gold standard to compare with the surrogate predictions. Fig. 1 shows an overview of the methodology used in this study.

### 2.1. Database

Experimental gait trials of four subjects, implanted with unilateral knee prosthesis (three male and one female, height: $168.3 \pm 2.6$ cm; mass: $69.2 \pm 6.2$ kg), were obtained from a previously published repository [https://simtk.org/home/kneeloads; accessed on June 2013]. All subjects were implanted with sensor-based knee prostheses that have been specifically manufactured for in vivo measurement of knee joint forces [30]. The database included three dimensional ground reaction

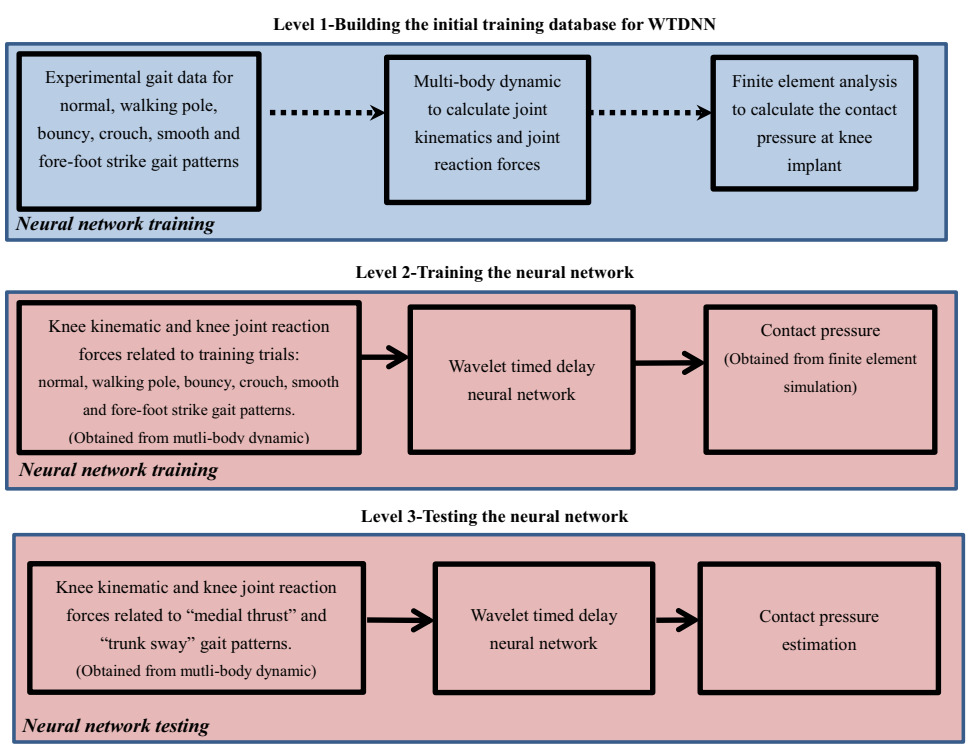


**Fig. 1.** Schematic description of the proposed methodology.

forces (GRFs) (force-plates, AMTI, Watertown, MA, USA) and marker trajectory data obtained from a six-camera Vicon motion analysis system (Oxford Metrics, Oxford, UK) with a modified version of the University of Western Australia (UWA) marker set, with additional markers on the toes [31]. All the gait trials were recorded over ground at a self-selected pace. For a complete description of walking trials see [30].

Gait trials contained *normal*, *walking pole*, *bouncy*, *crouch*, *fore-foot strike* and *smooth* patterns (107 trials) as well as *medial thrust* and *trunk sway* patterns (37 trials). In brief, *medial thrust* pattern included a slight decrease in pelvis obliquity and a slight increase in pelvis axial rotation and leg flexion compared to *normal* gait [11]. In *trunk sway*, subjects (except subject 4) walked with an increased lateral lean of trunk in frontal plane over the standing leg [10]. Since "*medial thrust*" and "*trunk sway*" have been objectively designed for knee rehabilitation purposes, in the rest of this study, *normal*, *walking pole*, *bouncy*, *crouch*, *fore-foot strike* and *smooth* are refereed as "training data" which were used to train the surrogate model (neural network) and "*medial thrust*" and "*walking pole*" are referred as " prediction data" which were aimed to be predicted by the neural network. A gait cycle was defined as the time interval between foot strike of one leg to the following foot strike of the same leg [32]. Subsequently two complete gait cycles were picked up for each trial, leading to a total of 288 data sets (144 trials $\times$ two gait cycles). Training gait cycles (214 data sets) were used to train the surrogate model. The remaining 74 gait cycles, associated with rehabilitation programs, were then used as test data space to evaluate the performance of the surrogate model (see Fig. 1).

### 2.2. Multi-body dynamics simulation

Experimental GRFs and marker trajectories were imported into the three-dimensional multi-body simulation software: AnyBody Modeling System (version 5.2, AnyBody Technology, Aalborg, Denmark). A lower extremity musculoskeletal model was used in AnyBody software based on the University of Twente Lower Extremity Model (TLEM) [33]. The TLEM model is available in the published repository of AnyBody software. This model included approximately 160 muscle units as well as thigh, patella, shank and foot segments. Hip joint was modeled as a spherical joint with three degrees of freedom (DOF): flexion–extension, abduction–adduction and internal–external rotation. Knee joint was modeled as a hinge joint with only one DOF for flexion–extension and universal joint was considered for ankle–subtalar complex. Since the assumptions of the simplified knee joint and rigid multi-bodies were made, the detailed knee implant was not considered in the multi-body dynamic analysis. For each subject, the generic musculoskeletal model was scaled based on a Length–Mass–Fat scaling law in which body mass, body height and segment length were taken into account. Segment lengths were calculated according to the markers' coordination in an optimization routine in which the model was scaled such that the differences between "model marker" and the "experimental marker" trajectories were minimized. Detailed information about scaling techniques for a musculoskeletal model can be found in [34–36]. The scaled model was then recruited in an inverse dynamics approach in AnyBody software in which joint kinetics and muscle forces were calculated. Joint kinetics were calculated from equilibrium equations. Muscle forces were calculated as an optimization problem in which muscle recruitments, based on a cubic polynomial muscle recruitment criterion, were computed in order to minimize the maximum muscle activities subject to equilibrium constraints and positive muscle force constraints [34,37]. Knee flexion–extension angle and three dimensional knee reaction forces, aligned in medial–lateral, proximal–distal and anterior–posterior directions, were calculated for each gait cycle. Calculated knee kinematic and kinetic waveforms were then normalized to 100 samples, through the linear interpolation technique (MATLAB v. 2009, The MathWorks, Inc., Natick, MA,USA), representing one complete gait cycle from heel strike (0%) to toe-off (100%) (Fig. 2). Normalized knee kinematic and kinetic waveforms served as the boundary condition and loading profiles required for FEA.

### 2.3. Explicit finite element simulation

The tibiofemoral knee implant of the subject was modeled in the commercial finite element package; ABAQUS/Explicit (version 6.12 Simulia Inc., Providence, RI, USA) using a computer aided design (CAD) model of a typical fixed bearing posterior stabilized total knee implant. The knee implant consisted of two main parts; femoral component and tibia insert (Fig. 3). Rigid body assumptions were applied to both femoral and tibia insert components, with a simple linear elastic foundation model defined between the two contacting bodies [38].

Modified quadratic tetrahedron 10-node elements (C3D10M) were used to mesh the tibiofemoral knee implant in ABAQUS. Convergence was tested by decreasing the edge length of elements from 8 mm to 0.5 mm in five steps (8, 4, 2, 1, and 0.5 mm). The solution converged to a mesh with the average element edge length of 1 mm. The converged mesh contained over 86000C3D10M elements to represent the femoral component (4200 elements with 6700 nodes) and the tibia insert (4400 elements with 6600 nodes). Further increase in the mesh density resulted in minor changes to the calculated contact pressure ($\leq 5\%$). The physical interaction between these two components was taken into account as a surface-to-surface contact (femur as the master surface and tibia as the slave surface) through a penalty based approach and an isotropic friction coefficient of 0.04 [38,39]. The tibia insert was constrained in all available DOFs and the femoral component was only allowed for flexion–extension under the three dimensional load. Three dimensional knee loadings and knee flexion angle were obtained from multi-body dynamic analysis (Fig. 2). The FE model calculated the contact pressure at each node for each time increment. Although the contact pressures were calculated on the whole tibia surface, only medial tibia compartment of the knee implant was focused to illustrate the proposed methodology since this part is mainly prone to higher contact pressure during gait [40].

### 2.4. Field output construction

Using FEA, the time history of spatial contact pressures were calculated at the nodes in contact, however only the maximum values of nodal pressures over the entire gait were concerned in this study. Each gait cycle was depicted as a topographic outline in which the maximum contact pressures and the corresponding contact regions (contact nodes) were highlighted over the entire gait cycle. In order to form such a topographic outline, an output field was established in the following three steps:

*Step* 1. *Define the widest potential contact region (PSURF)*: All of the achievable contact contours within the entire simulation frames were combined over all the training gait cycles to construct the widest potential contact zone called PSURF (Fig. 4). Indeed PSURF was a vector of node numbers that represented a comprehensive collection of potential contact nodes.

*Step* 2. *Calculate the maximum values of contact pressures on PSURF*: Each training gait cycle was outlined through the maximum values of contact pressures associated with the nodes in PSURF. Maximum contact pressure values were then arranged in a vector and treated as a pressure signal for that gait cycle. Pressure signals were combined over all training gait cycles to form a matrix called CPRESS-MAX in which each column was allocated for one training gait cycle (Fig. 4).

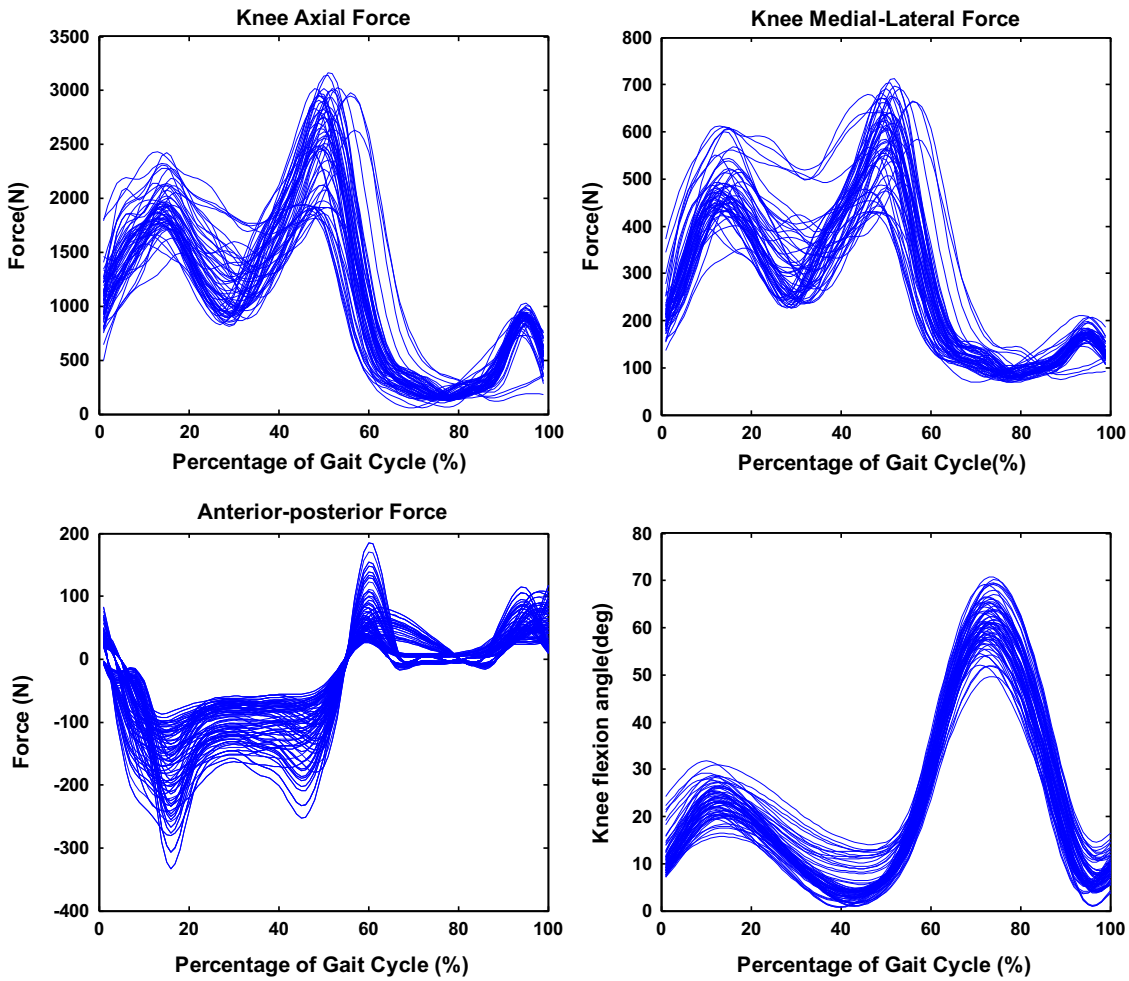


**Fig. 2.** Normalized knee joint force and flexion angle (served as FEA boundary condition and load).

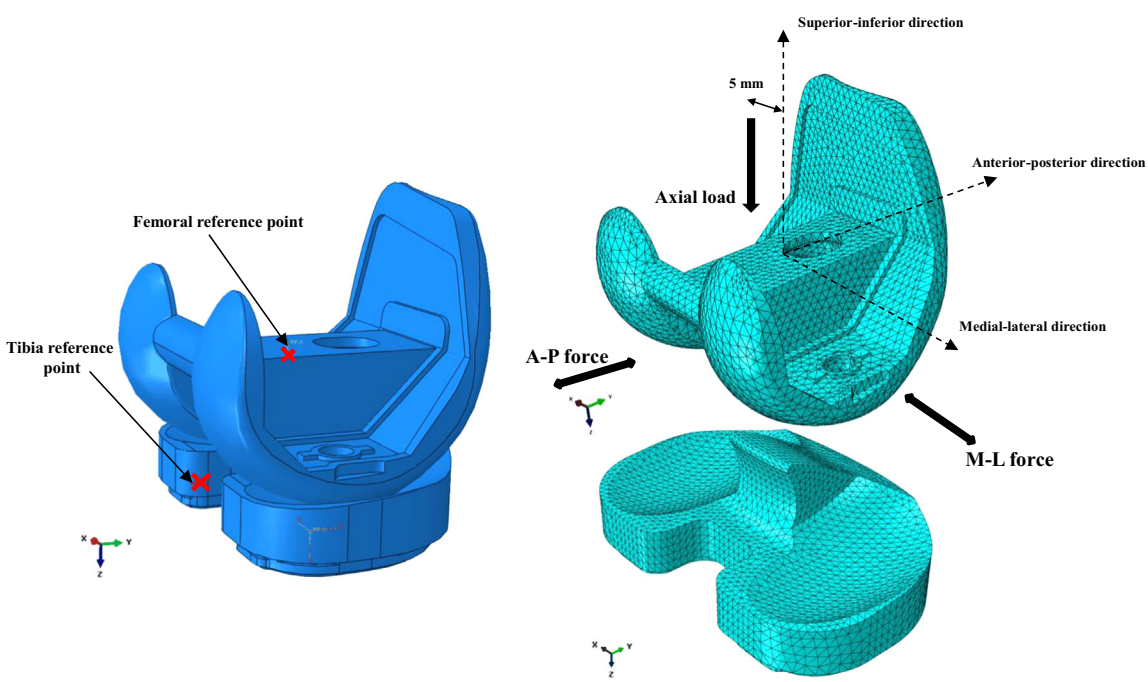


**Fig. 3.** CAD model of the fixed bearing posterior stabilized knee implant which was used in this study.

*Step* 3. *Partition the PSURF into five sub-regions:* The pressure signal, defined for each gait cycle, contained an overall description of that gait cycle including a variety of different pressure values ranging from low to high values associated with low and high pressure contact regions which occurred within that gait cycle. In order to reduce the variability of network's output and increase the

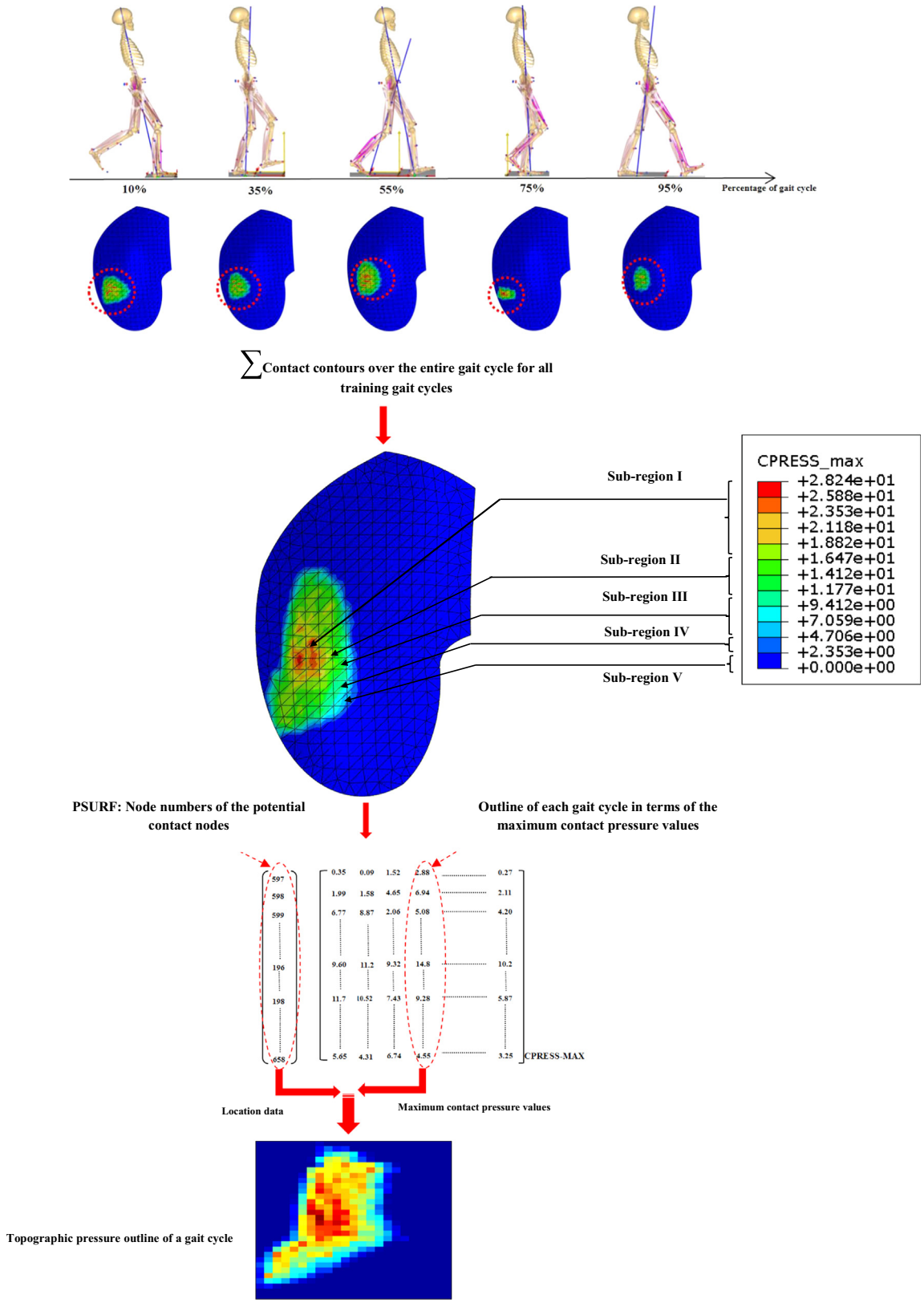


**Fig. 4.** PSURF and CPRESS_MAX matrix; PURF contained a comprehensive collection of potential contact nodes over all training gait cycles. Each gait cycle was represented with the maximum contact pressure values associated with the nodes in PSURF.

prediction ability of the proposed surrogate model, PSURF (contact nodes) was divided into five sub-regions: *sub-region I* (contact pressure > 16 MPa), *sub-region II* (10 MPa < contact pressure ≤ 16 MPa), *sub-region III* (2 MPa < contact pressure ≤ 10 MPa), *sub-region IV* (0.5 MPa < contact pressure ≤ 2 MPa) and *sub-region V* (0 MPa < contact pressure ≤ 0.5 MPa). For each contact node

belonged to PSURF, the class membership probability to each sub-region was determined; for example for *sub-region I*

$$P^{I}(node_i) = \frac{\text{total number of gait cycles in which the maximum contact pressure on node } i > 16 \text{ MPa}}{\text{total number of training gait cycles}} \quad node_i \in PSURF \tag{1}$$

Accordingly, using the CPRESS-MAX matrix, five membership probability values were calculated for each node as $P^{I}(node_i)$, $P^{II}(node_i)$, $P^{III}(node_i)$, $P^{IV}(node_i)$, $P^{V}(node_i)$. Each node was assigned to the sub-region with the highest membership probability. In other words, the maximum values of contact pressure for a node in *sub-region I* were above 16 MPa in most of the training trials while a node in *sub-region V* mostly had maximum contact pressure lower than 0.5 MPa (Fig. 5). Upper and lower pressure boundaries of sub-regions were chosen so as to have sub-regions with equal numbers of nodes as far as possible.

### 2.5. Surrogate model: wavelet time delay neural network

Due to the advantages of time delay neural network (TDNN) for real-time estimation of contact stress [28] and major drawbacks of this structure stemmed from global activation functions [29,41,42], a three-layer wavelet time delay neural network (WTDNN) was developed in the present study. This structure had a similar architecture with TDNN: a feed-forward neural network with a tapped delay line, added to the input layer, which enabled the network to store a short-time history of input patterns [43]. In each layer, neurons were connected to the neurons of the next layer via numeric values (weights). Thus a weighted sum of all inputs was fed into each hidden neuron where an activation function acted on this weighted sum to produce the hidden neuron's output. Although hidden neurons are generally activated with a global activation function, in the present structure hidden neurons were activated with wavelets (Fig. 6). Each input node was related to each hidden neuron, with a special value of shift, scale and input weight parameters. Therefore, each of the hidden neurons was activated with a multi-dimensional wavelet defined as the tensor product of one-dimensional wavelets corresponding to each input as below [18]:

$$\psi_i(x_1, x_2, x_3, \ldots, x_{N_i}) = \prod_{k=1}^{Ni} \psi\left(\frac{x_k w_{ik} - t_{ik}}{\lambda_{ik}}\right) \quad k = 1, 2, \ldots, N_i; \quad i = 1, 2, 3, \ldots, M \tag{2}$$

In which $\psi(t)$ is Daubechies4 (db4) wavelet function; $N_i$ indicates the number of input nodes, $M$ is the number of hidden neurons and $w_{ik}$,$t_{ik}$ and $\lambda_{ik}$ are the input weight, shift and scale parameters relating $k$th input to the $i$th hidden neuron respectively. It should be pointed out that each hidden neuron acted on each input signal by a shifted and scaled version of mother wavelet (db4). The outputs of hidden neurons were fed in to the output neuron via special values of weights led to a $1 \times M$ output weight matrix. Consequently the output of the proposed network was defined as follows:

$$y = \sum_{i=1}^{M} w_i \psi_i(x_1, x_2, x_3, \ldots, x_{N_i}) + \bar{y} \quad i = 1, 2, \ldots, M; \tag{3}$$

where $\psi_i(x_1, x_2, x_3, \ldots, x_{N_i})$ is defined in Eq. (2) and $w_i$ is the output weight relating $i$th hidden neuron to the output node and $\bar{y}$ is the bias. Five groups of parameters (input weights, shift, scale, output weights and bias value) were adjusted in WTDNN training as required in the above equations. It should be pointed out that unlike the conventional neural networks; in the case of WTDNN, it was important to initialize the adjustable parameters before training in order to ensure that the daughter wavelets (shifted and scaled versions of mother wavelet) covered the entire input data space. Therefore, the WTDNN was trained within the two main steps; *first* the adjustable parameters were initialized, see

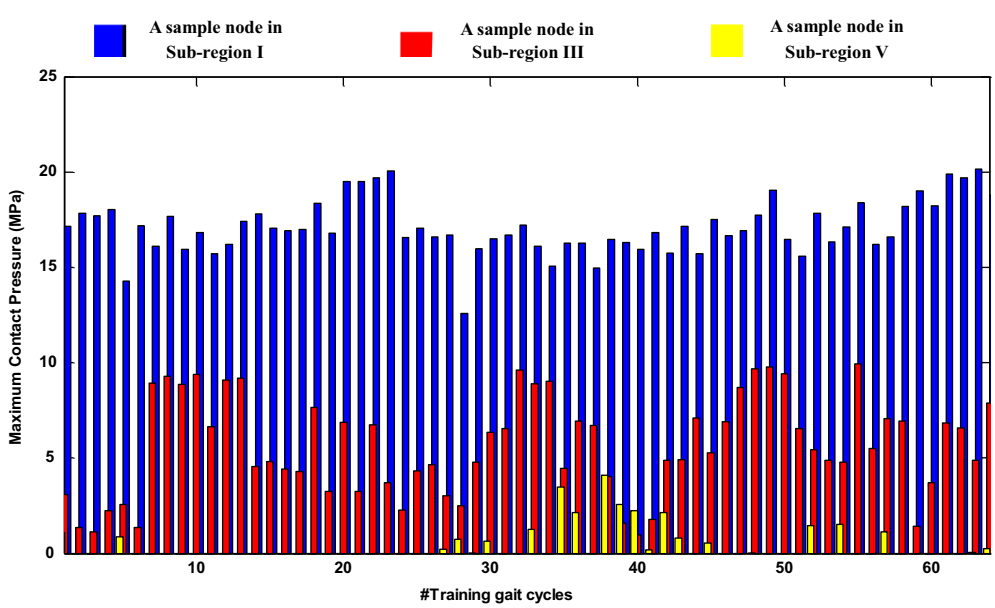


**Fig. 5.** Three sample nodes from PSURF belonged to *sub-region I*, *sub-region III* and *sub-region V*. The maximum values of contact pressure for the node in *sub-region I* were mostly above 16 MPa whilst the node in *sub-region III* essentially experienced maximum contact pressure values in the range of 2–10 MPa.

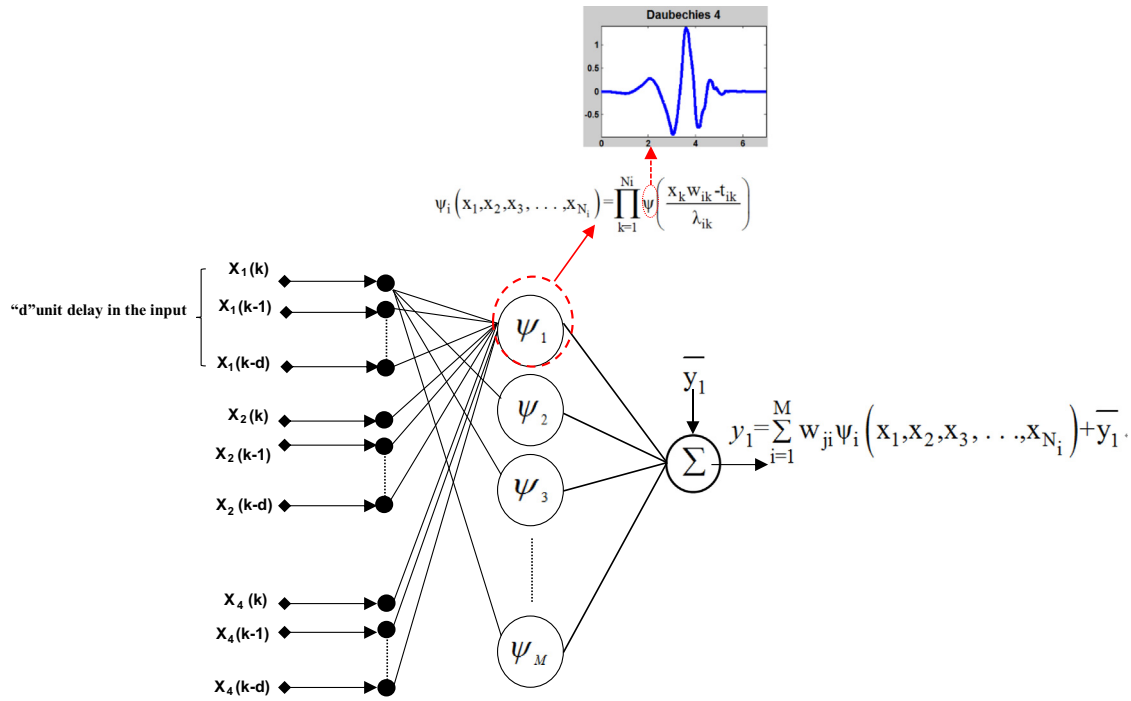


**Fig. 6.** A schematic block diagram of the proposed wavelet time delay neural network with four inputs ($Ni=4$) and one output.

[44]; *second*, a MATLAB script (v. 2009, MathWorks, Inc., Natick, MA, USA) was developed to train the WTDNN based on scaled conjugate gradient algorithm (SCG). For a complete description of SCG one can refer to [45].

Five parallel WTDNNs served to predict the maximum contact pressure values at the nodes in contact; one WTDNN was allocated to predict the pressure distribution of each sub-region. Each network had one input layer with four inputs ($N_i=4$) including knee flexion angle plus three dimensional knee reaction forces. In this approach, the maximum contact pressure values associated with each sub-region were arranged as a vector and treated as a pressure signal (output signal). Thus, each WTDNN had a single output layer with one output neuron and the input data space (knee flexion angle and knee reaction forces) were re-sampled and interpolated to have an equal size with the output signal.

Training gait trials, including *normal*, *bouncy*, *crouch*, *smooth*, *walking pole* and *forefoot strike* patterns of four subjects, were used to train the generic networks while testing trials (*medial thrust* and *trunk sway*) were not included in the network training procedure and were only used to test the performance of the trained WTDNNs. Training data space was randomly divided into three main subsets; 70% for training, 15% for validation and 15% to test the generalization ability of the trained network. The optimal numbers of hidden neurons and training epochs were determined due to the network prediction error on validation and test subsets. Hidden neurons and training epochs were increased until adding more hidden neurons/training epochs would increase the network prediction error on the test subset due to over-fitting. The error goal was set to 0.0001 and the training algorithm was continued to achieve the error goal or until the maximum epochs were reached. The optimal tapped delay was also determined by trial and error. All of the above analyses were conducted in MATLAB. According to [46], the network was trained and run 100 times for each test data set (testing gait cycle) and the average of these 100 runs was considered as the network prediction for that test data set. WTDNNs predictions were then combined together and assigned to the corresponding contact regions (PSURF) to form the topography of maximum contact pressure distribution. The performance of the WTDNNs were benchmarked against the FEA (gold standard) in terms of root mean square error ($\overline{RMSE}$) and its normalized percentage ($\overline{NRMSE}$) as well as Pearson correlation coefficient ($\overline{\rho}$).

## 3. Results

### 3.1. Maximum contact pressure prediction on sub-regions

The widest potential contact region (PSURF) contained a total of 500 nodes. The PSURF region was then divided into five partitions from high-pressure sub-region (*sub-region I*) to low-pressure sub-region (*sub-region V*) with 101 nodes in *sub-region I*, 102 nodes in *sub-region II*,109 nodes in *sub-region III*, 46 nodes in *sub-region IV* and 141 nodes in *sub-region V*. For each sub-region, the pressure values estimated by WTDNN were compared with the corresponding values obtained from FEA for *medial thrust* (Fig. 7) and *trunk sway* (Fig. 8) rehabilitation patterns. Table 1 summarizes the structure of the networks and the accuracy of predictions in terms of $\overline{RMSE}$, $\overline{NRMSE}$(%) and Pearson correlation ($\overline{\rho}$). For *medial thrust* prediction, cross correlation values ranged from $\overline{\rho}=0.89$ to $\overline{\rho}=0.97$ and all of the errors ($\overline{NRMSE}$) were less than 14% compared to FEA results. The predicted pressure signal of *sub-region I* had the lowest error of $\overline{NRMSE}=6.3\%$ with the correlation coefficient above $\overline{\rho}=0.95$. The predicted pressure signal of *sub-region II* had the highest error of $\overline{NRMSE}=13.2\%$ with the correlation coefficient of $\overline{\rho}=0.89$. For *trunk sway* prediction, errors were slightly increased compared to the corresponding sub-regions of *medial thrust* pattern since subject 4 did not undergo *trunk sway* rehabilitation and predictions were averaged on a fewer number of subjects. Cross correlation coefficients ranged from $\overline{\rho}=0.81$ to $\overline{\rho}=0.97$ and all of the $\overline{NRMSE}$ values were less than 15%. The lowest prediction error was related to *sub-region I* ($\overline{NRMSE}=7.3\%$, $\overline{\rho}=0.95$) and the highest error occurred in *sub-region V* ($\overline{NRMSE}=14.3\%$, $\overline{\rho}=0.81$).

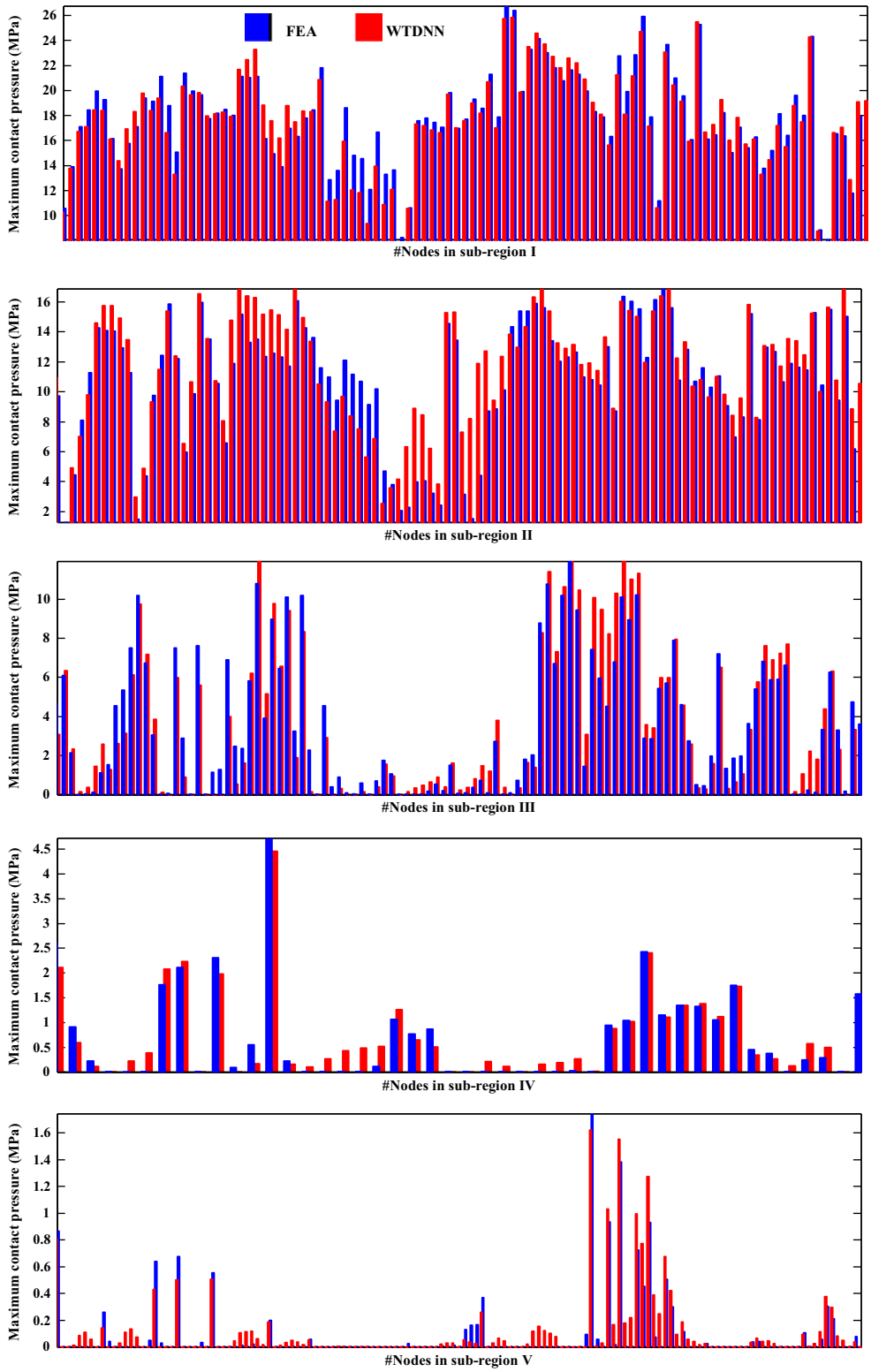


**Fig. 7.** A sample comparison between WTDNN estimations (red bars) and FEA calculations (blue bars). Note maximum contact pressure values were associated with medial thrust gait pattern for sub-region I–V. (For interpretation of the references to color in this figure legend, the reader is referred to the web version of this article.)

### *3.2. Topographic representation of maximum contact pressure distribution*

For each subject, five pressure signals were obtained from WTDNNs and were combined to reconstruct the complete pressure signal of a gait cycle. For each subject, pressure signals were then averaged over the testing gait cycles of each pattern (*medial thrust* or *trunk sway*) to generate an overall estimation of that rehabilitation pattern. Consequently WTDNN predictions and FEA calculations were then assigned to the corresponding contact regions (PSURF) to form the topographic representation of the maximum contact pressure distribution. Figs. 9 and 10 present the topographic outline of *medial thrust* and *trunk sway* rehabilitation patterns for each subject. The quantitative comparison of the

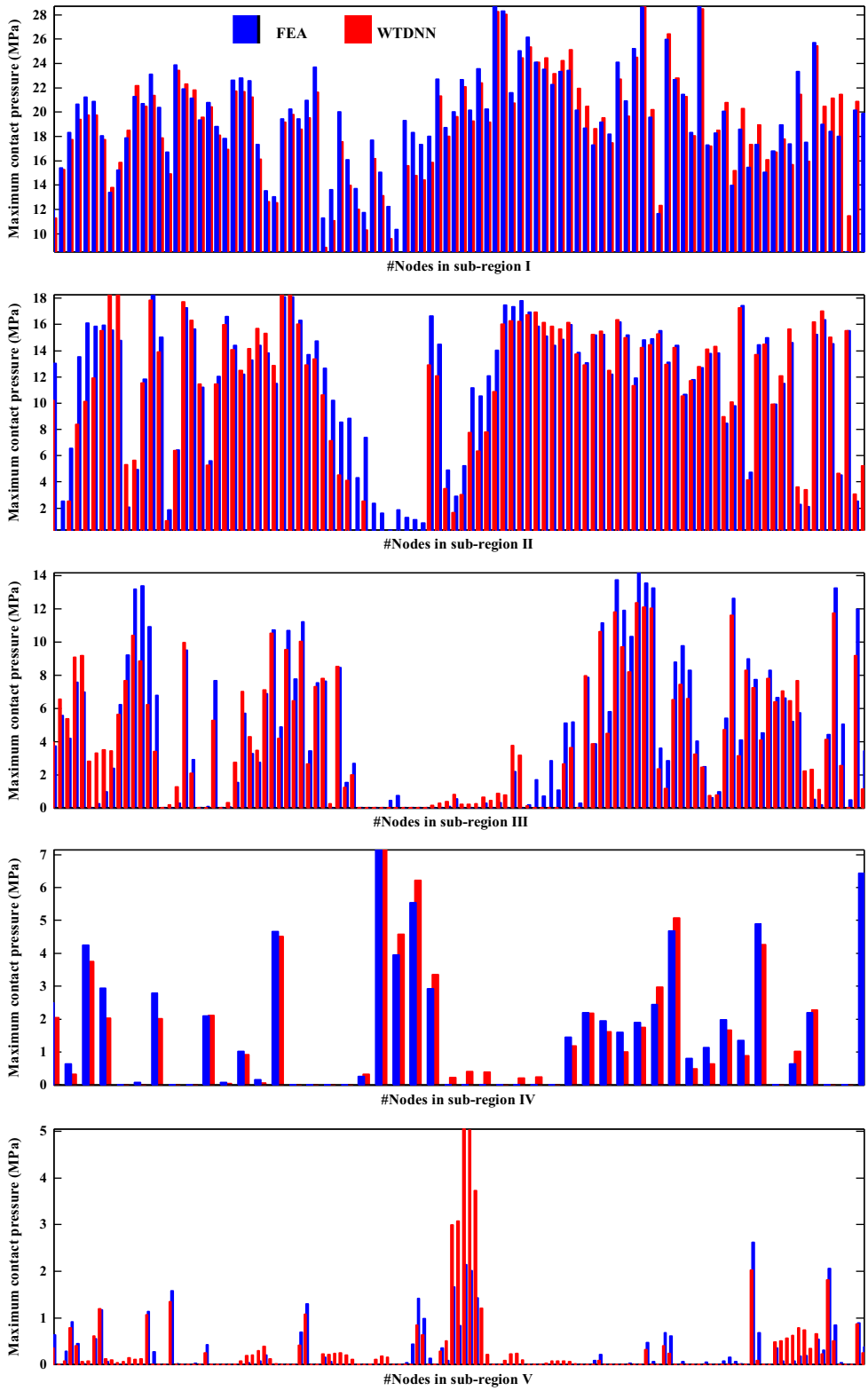


**Fig. 8.** A sample comparison between WTDNN estimations (red bars) and FEA calculations (blue bars). Note maximum contact pressure values were associated with trunk sway gait pattern for sub-region I–V. (For interpretation of the references to color in this figure legend, the reader is referred to the web version of this article.)

predicted topographies (Table 2) shows that WTDNN could predict the maximum contact pressure distributions to a high level of accuracy for *medial thrust* ($\overline{RMSE}=1.7$ MPa, $\overline{NRMSE}=6.2\%$ and $\overline{\rho}=0.98$) and *trunk sway* ($\overline{RMSE}=2.6$ MPa, $\overline{NRMSE}=9.3\%$, $\overline{\rho}=0.96$). The simulation time for a complete gait cycle, discretized into 100 increments, was approximately 40 min for the FE model, compared to 30 s for the WTDNN on the same CPU (Dual-Core CPU 2.93 GHz, 4 GB RAM).

## 4. Discussion

Incorporating the localization property of wavelets and temporal pattern prediction of time delay neural networks, wavelet time delay neural network was developed as a novel surrogate model which provided a real-time evaluation of knee rehabilitation programs in terms of maximum contact pressure distribution.

**Table 1**
WTDNN structures which were allocated to each sub-region. Each network had four inputs (knee flexion and three dimensional knee reaction forces) and one single output (the contact pressure signal). For each sub-region, prediction errors were averaged over four subjects to represent an overall evaluation of the WTDNN prediction ability on a specific pressure sub-region.

| | **Sub-region** | **Cluster-specific network Time delay, [hidden layer1, hidden layer 2], epochs** | $\overline{RMSE}$(***MPa***) | $\overline{NRMSE}$ (%) | $\overline{\rho}$ |
|---|---|---|---|---|---|
| Medial thrust | Sub-region I | [0 5], [35], 3000 | 1.2 | 6.3 | 0.96 |
| | Sub-region II | [0 3], [30], 3000 | 2.0 | 13.2 | 0.89 |
| | Sub-region III | [0 5], [25], 3000 | 1.3 | 11.0 | 0.94 |
| | Sub-region IV | [0 3], [20], 1000 | 0.3 | 5.2 | 0.97 |
| | Sub-region V | [0 3], [20], 1000 | 0.1 | 5.8 | 0.94 |
| Trunk sway | Sub-region I | [0 5], [30], 3000 | 1.5 | 7.3 | 0.95 |
| | Sub-region II | [0 5], [25], 3000 | 2.4 | 13.1 | 0.94 |
| | Sub-region III | [0 5], [25], 3000 | 1.6 | 11.4 | 0.94 |
| | Sub-region IV | [0 3], [20], 1000 | 0.5 | 7.4 | 0.97 |
| | Sub-region V | [0 3], [18], 2000 | 0.5 | 14.3 | 0.81 |

The generalization ability of the proposed structure was tested by predicting the maximum contact pressure distribution associated with two rehabilitation patterns for four different subjects. To build the initial training database, required to train the WTDNN surrogate, a total of 214 FE simulations were performed. This initial step was time consuming; however, once WTDNN was developed, it facilitated the simulation of hundreds of analyses in a fraction of the time required to run the original FE model and therefore released the necessity of repeating the time consuming calculations.

### 4.1. Topographic outline of maximum contact pressure distribution

Previous attempt to predict contact pressure through artificial intelligence has been limited to a one-by-one mapping from "force" data space into the resultant "contact stress" using a large neural network structure for a simplified contact model and for a small number of data sets (25 sets) including only uniform levels of loading [28].Therefore, the actual feasibility of the proposed TDNN did not consider realistic gait. Indeed Lu et al. proposed an approach which may not be practical in realistic applications since the size of the required network will increase rapidly as the contact model includes further number of elements. Additionally, in clinical rehabilitation, the time history of spatial contact pressure distribution is not needed and only *maximum* contact pressures are of interest. Therefore, to release the necessity of a large-structure neural network, a topographic outline of contact pressures was defined to highlight the maximum nodal contact pressures and the corresponding contact nodes over a complete gait cycle. To form this topographic outline, the widest contact zone (PSURF) was defined by including a comprehensive collection of potential contact nodes over all training gait cycles. It should be pointed out that PSURF was established from the training gait trials (training data space). However due to the nature of probability and the mathematical principle of induction, for a new walking pattern (rehabilitation strategy), the probability of contact on a node which was not included in PSURF would be very low, and the probability of high contact pressure occurrence on such a node would be even less. As a result, predicting the maximum contact pressures associated with the nodes in PSURF would suffice as a real-time evaluation of the rehabilitation programs in terms of the resultant contact pressures.

For each gait cycle, the maximum contact pressure values associated with the contact nodes (PSURF) were arranged as a vector and treated as the pressure signal to be predicted by a single-output neural network. This pressure signal contained a large variety of different values from 0 MPa associated with a low pressure contact region to 31 MPa for a high pressure contact region that might occur during a gait cycle. In order to improve the prediction ability of the network, PSURF was partitioned into five sub-regions based on the probability of contact pressure levels that might occur on each sub-region. For example those nodes that mostly experienced contact pressures lower than 0.5 MPa over the training gait cycles were classified as the low pressure sub-region (*sub-region V*). From a technical point of view, nodes belonged to a sub-region would likely experience similar values of maximum contact pressure for a new walking condition (rehabilitation trial). Thus, partitioning the PSURF reduced the amount of variability in the network output which enhanced the prediction ability of the network. The maximum pressure values of nodes belonged to each sub-region were then arranged in a pressure sub-signal and assigned to the output of the surrogate model.

### 4.2. Wavelet time delay neural network

Time delay neural network (TDNN) has been used successfully for real-time estimation [47,48]. Particularly Lu et al., has reported the superiority of TDNN compared to feed forward structure to predict contact stress [28]. However, a major drawback of traditional neural networks (e.g. TDNN) is that hidden neurons are activated by global infinite functions. Therefore, local data structures are discarded in learning process [41]. In addition, the initial weights are adjusted randomly at the beginning of the training algorithm which can slow down the training process [29]. Another disadvantage is that the network may fall in to a local minimum during the training procedure so the network output never converges to the target [42].To release the aforementioned disadvantages, wavelet has been introduced to the neural network structure [49]. Recent studies have shown that replacing the global infinite activation functions with local wavelets increases the functionality of the network in terms of prediction accuracy [18,50,51]. Hence, wavelet was embedded in the structure of the surrogate model. Table 3 summarizes a systematic comparison between the present study and the previously published research by Lu et al. [28].

### 4.3. Limitations and future research directions

There are a number of limitations in this study. First, the present study used the CAD model of a typical implant [52–55] which had different geometry compared to the original prosthesis by which the subjects were implanted. In fact subjects were implanted with a sensor-based prosthesis that was specifically manufactured to measure in vivo knee loadings [30]. Although the geometry of knee prosthesis can alter the absolute values of contact pressures calculated in FEA, the present study did not aim to report the absolute values of pressure and the proposed methodology will be equally applicable to any implant geometries.

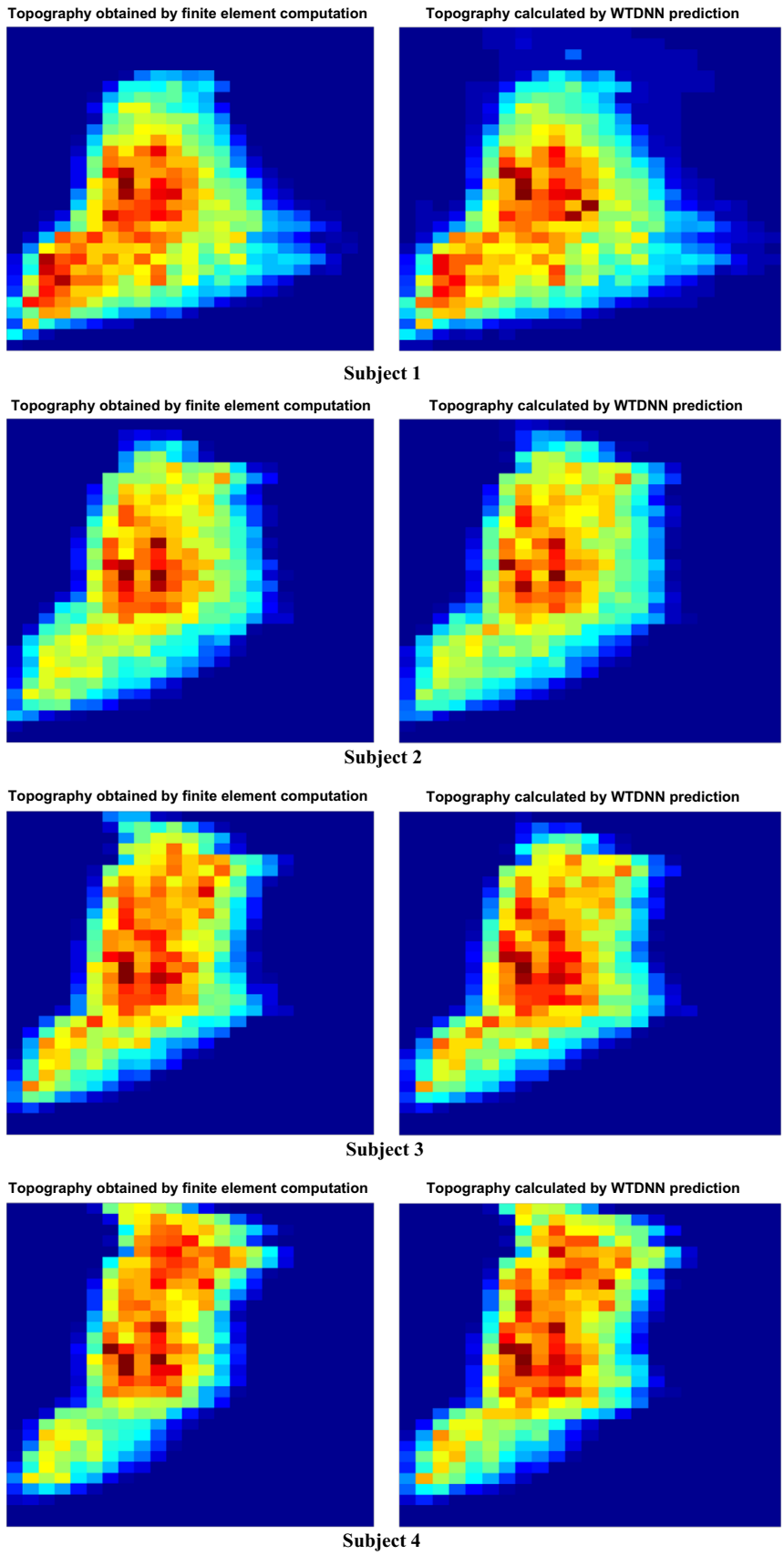


**Fig. 9.** Finite element computations and WTDNN predictions were settled in the corresponding contact nodes (preserved in PSURF) to form a topographic outline of maximum contact pressure distribution for *medial thrust* rehabilitation.

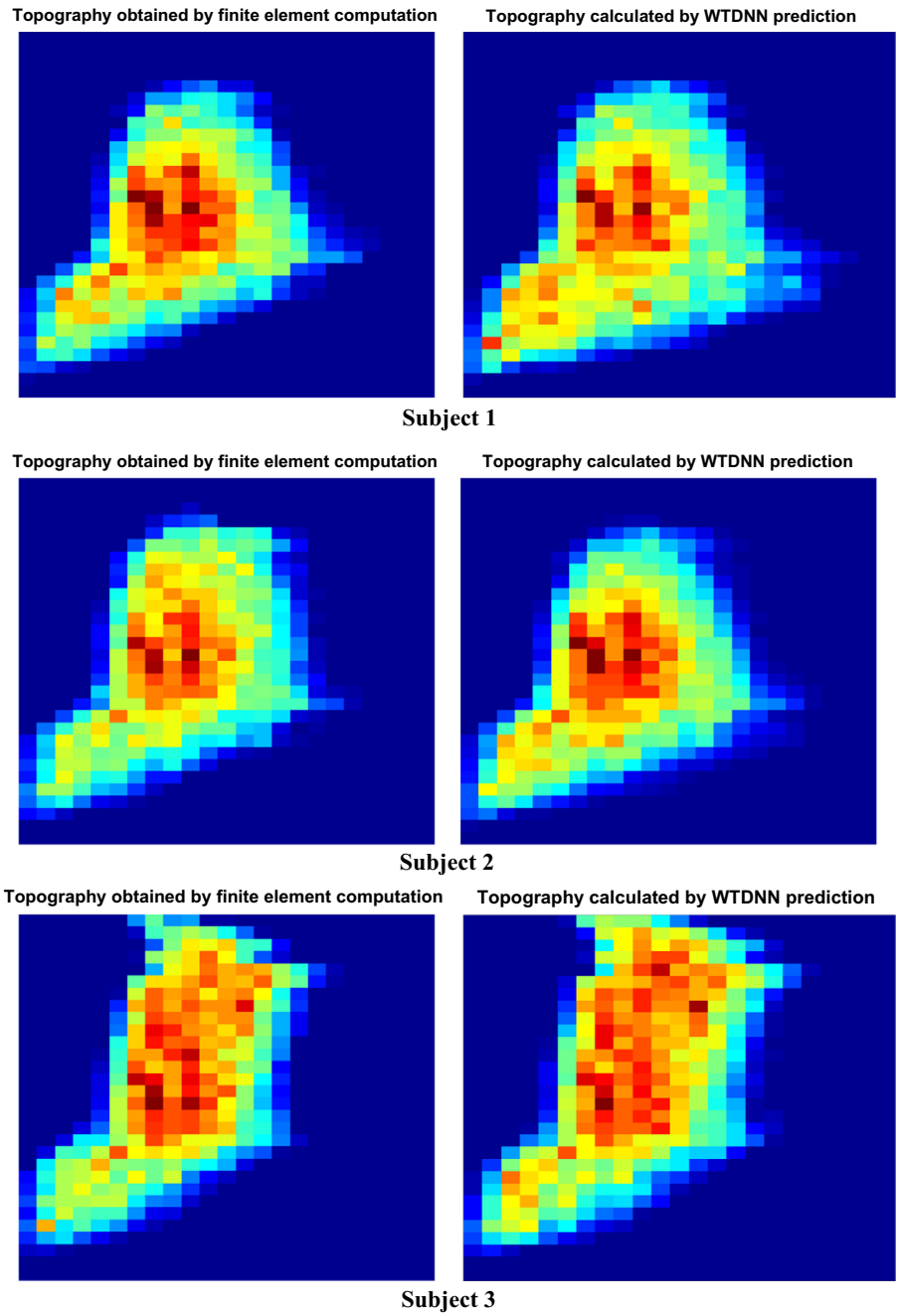


**Fig. 10.** Finite element computations and WTDNN predictions were settled in the corresponding contact nodes (preserved in PSURF) to form the topographic outline of maximum contact pressure distribution for *trunk sway* rehabilitation. Subject 4 did not undergo *trunk sway* rehabilitation.

**Table 2**
Prediction accuracy of WTDNN for topographic outlines of *medial thrust* and *trunk sway* patterns related to each subject.

| | **Subject** | $\overline{RMSE}(MPa)$ | $\overline{NRMSE}$**(%)** | $\overline{\rho}$ |
|---|---|---|---|---|
| Medial thrust | Subject 1 | 1.7 | 5.7 | 0.99 |
| | Subject 2 | 1.5 | 5.0 | 0.98 |
| | Subject 3 | 1.9 | 7.3 | 0.97 |
| | Subject 4 | 1.8 | 6.6 | 0.98 |
| | **Average** | 1.7 MPa | 6.2% | 0.98 |
| Trunk sway | Subject 1 | 2.6 | 9.1 | 0.96 |
| | Subject 2 | 2.4 | 8.2 | 0.95 |
| | Subject 3 | 2.7 | 10.4 | 0.97 |
| | **Average** | 2.6 MPa | 9.3% | 0.96 |

Second, rigid body constraints were applied in the finite element simulation to both femoral component and tibia insert. In fact Halloran et al. showed that rigid body analysis of the tibiofemoral knee implant can calculate contact pressure and contact area in an acceptable consistence with a full deformable analysis [38] whilst rigid body simulation would be much more time-efficient. Accordingly, rigid body constraints were applied to both femoral and tibia insert to produce the required training input–output data sets with a reasonable computational cost. This is consistent with the present multi-body dynamics analysis that no detailed modeling on the knee implant was included. The present approach can also be trained based on the contact pressure and von Mises stress obtained from a deformable simulation of knee implant. Third, knee joint was modeled with

**Table 3**
A comparison between the present study and a previously published research.

| Study | Network architecture | Structure [inputs, hidden neurons, outputs] | #Training datasets | #Test data sets | Output field | Issues |
|---|---|---|---|---|---|---|
| Lu et al. [26] | FFANN | [1200, 80, 400] | 20 sets | 5 sets | Spatial contact stress distribution | Increasing the number of elements in the contact model enlarges the structure of the surrogate |
| | TDNN | [1200, 280, 400] | 20 sets | 5 sets | Spatial contact stress distribution | |
| Present study | WTDNN | [4, 20, 1] | 214 sets | 74 sets | Maximum contact pressure distribution | Increasing the number of elements in the contact model increases the size of the pressure signal but does not enlarge the network structure. |

only one DOF (flexion–extension). Although six DOFs are possible for the knee joint, the dominant movement of the knee joint takes place in the sagittal plane and knee joint has been mostly simplified as a hinge joint [11,56,57]. This is also consistent with our musculoskeletal model (TLEM model) in which knee joint has been modeled as a hinge joint with one degree of freedom for flexion–extension.

The proposed WTDNN was trained based on a number of examples (training gait trials) to learn the input–output interaction and then generalized the relationship to new situations (testing gait trials). Thus it released the necessity of iterative computations and provided a concise real-time evaluation of rehabilitation treatments in terms of the resultant maximum contact pressure. Accordingly this intelligent surrogate model can also benefit sensitivity investigations where an output measure should be calculated repeatedly for a variety of perturbed inputs and time-consuming computation is required in each iteration. For example with a trained WTDNN it would be possible to investigate the effect of knee flexion angle on the resultant contact pressure at the medial tibiofemoral knee joint. Moreover, exploiting the artificial intelligence, it would be interesting and beneficial to predict the resultant contact pressure based on other available inputs such as ground reaction forces and/or gait kinematics. Using a trained WTDNN and telemetry facilities, it would be possible to provide a real-time monitoring of joint contact pressure for patients at home. Future research is required to explore the efficiency of the proposed approach for further numbers of subjects or other rehabilitation patterns. Training the proposed scheme with further numbers of subjects and employing additional inputs such as age or knee alignment in WTDNN creation process will be conducted in future studies.

## 5. Conclusion

Our study demonstrated the feasibility of wavelet time delay neural network to provide a real-time evaluation of knee rehabilitation strategies in terms of the resultant maximum contact pressure. The proposed network predicted the maximum contact pressure distribution at the medial tibia compartment of a knee implant using knee flexion angle and three dimensional knee reaction forces (inputs). All the prediction errors were less than 8% for *medial thrust* gait modification and below 11% for *trunk sway* gait modification. Accordingly the proposed approach could provide the topography of maximum contact pressure distribution in which the maximum values of pressures and the corresponding contact regions were demonstrated. These kinds of topographic outlines generate a cost-effective and real-time evaluation of rehabilitation patterns to recognize the likely high-pressure contact regions that might occur in clinical execution of knee rehabilitation strategies.

## Acknowledgments

This work was supported by the “Fundamental Research Funds for the Central Universities and National Natural Science Foundation of China [E050702 and E51323007]”. The authors gratefully acknowledge “ Grand Challenge Competition to Predict In Vivo Knee Loads” for releasing the experimental data. The authors would like to thank Shanghai Gaitech Scientific Instruments Co. Ltd. for supplementing Anybody software used in this study.

## References

[1] J.A. Barrios, K.M. Crossley, I.S. Davis, Gait retraining to reduce the knee adduction moment through real-time visual feedback of dynamic knee alignment, J. Biomech. 43 (2010) 2208–2213.
[2] B.J. Fregly, D.D. D'Lima, C.W. Colwell, Effective gait patterns for offloading the medial compartment of the knee, J. Orthop. Res. 27 (2009) 1016–1021.
[3] M.A. Hunt, M. Simic, R.S. Hinman, K.L. Bennell, T.V. Wrigley, Feasibility of a gait retraining strategy for reducing knee joint loading: increased trunk lean guided by real-time biofeedback, J. Biomech. 44 (2011) 943–947.
[4] J.C. van den Noort, I. Schaffers, J. Snijders, J. Harlaar, The effectiveness of voluntary modifications of gait pattern to reduce the knee adduction moment, Hum. Mov. Sci. (2013).
[5] S.M. Robbins, M.R. Maly, The effect of gait speed on the knee adduction moment depends on waveform summary measures, Gait & Posture 30 (2009) 543–546.
[6] Ardestani M.M., Chen Z., Wang L., Lian Q., Liu Y., He J., Li D., Jin Z., A neural network approach for determining gait modifications to reduce the contact force in knee joint implant, Medical Engineering & Physics, 36 (2014) 1253–1265.
[7] M.M. Ardestani, M. Moazen, Z. Jin, Gait modification and optimization using neural network–genetic algorithm approach: application to knee rehabilitation, Expert Syst. Appl. 41 (2014) 7466–7477.
[8] J. Willson, M.R. Torry, M.J. Decker, T. Kernozek, J. Steadman, Effects of walking poles on lower extremity gait mechanics, Med. Sci. Sports Exerc. 33 (2001) 142–147.
[9] A. Mündermann, C.O. Dyrby, D.E. Hurwitz, L. Sharma, T.P. Andriacchi, Potential strategies to reduce medial compartment loading in patients with knee osteoarthritis of varying severity: reduced walking speed, Arthritis Rheum. 50 (2004) 1172–1178.
[10] M. Hunt, T. Birmingham, D. Bryant, I. Jones, J. Giffin, T. Jenkyn, A. Vandervoort, Lateral trunk lean explains variation in dynamic knee joint load in patients with medial compartment knee osteoarthritis, Osteoarthritis Cartil. 16 (2008) 591–599.
[11] B.J. Fregly, J.A. Reinbolt, K.L. Rooney, K.H. Mitchell, T.L. Chmielewski, Design of patient-specific gait modifications for knee osteoarthritis rehabilitation, IEEE Trans. Biomed. Eng. 54 (2007) 1687–1695.
[12] R. Lafuente, J. Belda, J. Sanchez-Lacuesta, C. Soler, J. Prat, Design and test of neural networks and statistical classifiers in computer-aided movement analysis: a case study on gait analysis, Clin. Biomech. 13 (1998) 216–229.
[13] D.D. D'Lima, N. Steklov, B.J. Fregly, S.A. Banks, C.W. Colwell, In vivo contact stresses during activities of daily living after knee arthroplasty, J. Orthop. Res. 26 (2008) 1549–1555.
[14] B. Reggiani, A. Leardini, F. Corazza, M. Taylor, Finite element analysis of a total ankle replacement during the stance phase of gait, J. Biomech. 39 (2006) 1435–1443.
[15] C. Arsene, B. Gabrys, Probabilistic finite element predictions of the human lower limb model in total knee replacement, Med. Eng. Phys. 35 (2013) 1116–1132.
[16] D.D. Anderson, J.K. Goldsworthy, W. Li, M. James Rudert, Y. Tochigi, T.D. Brown, Physical validation of a patient-specific contact finite element model of the ankle, J. Biomech. 40 (2007) 1662–1669.

[17] S.C. Tadepalli, A. Erdemir, P.R. Cavanagh, Comparison of hexahedral and tetrahedral elements in finite element analysis of the foot and footwear, J. Biomech. 44 (2011) 2337–2343.
[18] M.M. Ardestani, X. Zhang, L. Wang, Q. Lian, Y. Liu, J. He, D. Li, Z. Jin, Human lower extremity joint moment prediction: a wavelet neural network approach, Expert Syst. Appl. 41 (2014) 4422–4433.
[19] S.E. Oh, A. Choi, J.H. Mun, Prediction of ground reaction forces during gait based on kinematics and a neural network model, J. Biomech. 46 (2013) 2372–2380.
[20] J. Favre, M. Hayoz, J.C. Erhart-Hledik, T.P. Andriacchi, A neural network model to predict knee adduction moment during walking based on ground reaction force and anthropometric measurements, J. Biomech. 45 (2012) 692–698.
[21] Y. Liu, S.-M. Shih, S.-L. Tian, Y.-J. Zhong, L. Li, Lower extremity joint torque predicted by using artificial neural network during vertical jump, J. Biomech. 42 (2009) 906–911.
[22] A.J. van den Bogert, T. Geijtenbeek, O. Even-Zohar, F. Steenbrink, E.C. Hardin, A real-time system for biomechanical analysis of human movement and muscle function, Med. Biol. Eng. Comput. (2013) 1–9.
[23] G. Campoli, H. Weinans, A.A. Zadpoor, Computational load estimation of the femur, J. Mech. Behav. Biomed. Mater. 10 (2012) 108–119.
[24] A.A. Zadpoor, G. Campoli, H. Weinans, Neural network prediction of load from the morphology of trabecular bone, Appl. Math. Model. (2012).
[25] N. Garijo, J. Martínez, J.M. García-Aznar, M.A. Pérez, Computational evaluation of different numerical tools for the prediction of proximal femur loads from bone morphology, Comput. Methods Appl. Mech. Eng. 268 (2014) 437–450.
[26] R. Hambli, Application of neural networks and finite element computation for multiscale simulation of bone remodeling, J. Mech. Eng. 132 (2010) 114502.
[27] R. Hambli, Numerical procedure for multiscale bone adaptation prediction based on neural networks and finite element simulation, Finite Elem. Anal. Des. 47 (2011) 835–842.
[28] Y. Lu, P.R. Pulasani, R. Derakhshani, T.M. Guess, Application of neural networks for the prediction of cartilage stress in a musculoskeletal system, Biomed. Signal Process. Control 8 (2013) 475–482.
[29] S.S. Haykin, Neural Networks and Learning Machines, Prentice Hall New York, 2009.
[30] B.J. Fregly, T.F. Besier, D.G. Lloyd, S.L. Delp, S.A. Banks, M.G. Pandy, D.D. D'Lima, Grand challenge competition to predict in vivo knee loads, J. Orthop. Res. 30 (2012) 503–513.
[31] T.F. Besier, D.L. Sturnieks, J.A. Alderson, D.G. Lloyd, Repeatability of gait data using a functional hip joint centre and a mean helical knee axis, J. Biomech. 36 (2003) 1159–1168.
[32] J. Perry, J.M. Burnfield, Gait Analysis: Normal and Pathological Function, Slack, Slack Incorporated, 1993.
[33] M.D. Klein Horsman, The Twente Lower Extremity Model: Consistent Dynamic Simulation of the Human Locomotor Apparatus, University of Twente, Enschede, Netherlands, 2007.
[34] N. Ali, M.S. Andersen, J. Rasmussen, D.G.E. Robertson, G. Rouhi, The application of musculoskeletal modeling to investigate gender bias in non-contact ACL injury rate during single-leg landings, Comput. Methods Biomech. Biomed. Eng. 17 (2013) 1602–1616.
[35] D.C. Frankenfield, W.A. Rowe, R.N. Cooney, J.S. Smith, D. Becker, Limits of body mass index to detect obesity and predict body composition, Nutrition 17 (2001) 26–30.
[36] P. Worsley, M. Stokes, M. Taylor, Predicted knee kinematics and kinetics during functional activities using motion capture and musculoskeletal modelling in healthy older people, Gait & Posture 33 (2011) 268–273.
[37] M. Damsgaard, J. Rasmussen, S.T. Christensen, E. Surma, M. de Zee, Analysis of musculoskeletal systems in the anybody modeling system, Simul. Model. Pract. Theory 14 (2006) 1100–1111.
[38] J.P. Halloran, A.J. Petrella, P.J. Rullkoetter, Explicit finite element modeling of total knee replacement mechanics, J. Biomech. 38 (2005) 323–331.
[39] A. Abdelgaied, F. Liu, C. Brockett, L. Jennings, J. Fisher, Z. Jin, Computational wear prediction of artificial knee joints based on a new wear law and formulation, J. Biomech. 44 (2011) 1108–1116.
[40] O. Schipplein, T. Andriacchi, Interaction between active and passive knee stabilizers during level walking, J. Orthop. Res. 9 (1991) 113–119.
[41] J.J. Cordova, W. Yu, X. Li, Haar wavelet neural networks for nonlinear system identification, IEEE International Symposium on Intelligent Control (ISIC), 2012 , pp. 276–281.
[42] P. Van Der Smagt, G. Hirzinger, Solving the ill-conditioning in neural network learning, Neural Networks: Tricks of the Trade, in: G. Orr, K.-R. Muller (Eds.), Lecture Notes in Computer Science 1524, Springer-Verlag, 1998, pp. 193–206.
[43] A. Waibel, T. Hanazawa, G. Hinton, K. Shikano, K.J. Lang, Phoneme recognition using time-delay neural networks, IEEE Trans. Acoust., Speech Signal Process. 37 (1989) 328–339.
[44] Q. Zhang, A. Benveniste, Wavelet networks, IEEE Trans. Neural Netw. 3 (1992) 889–898.
[45] M.F. Møller, A scaled conjugate gradient algorithm for fast supervised learning, Neural Netw. 6 (1993) 525–533.
[46] M.S. Iyer, R.R. Rhinehart, A method to determine the required number of neural-network training repetitions, IEEE Trans. Neural Netw. 10 (1999) 427–432.
[47] C. Wöhler, J.K. Anlauf, T. Pörtner, U. Franke, A time delay neural network algorithm for real-time pedestrian recognition, in: Proceedings of the International Conference on Intelligent Vehicle, Citeseer, 1998.
[48] M. Mishra, R. Derakhshani, G.C. Paiva, T.M. Guess, Nonlinear surrogate modeling of tibio-femoral joint interactions, Biomed. Signal Process. Control 6 (2011) 164–174.
[49] M.M. Ardestani, X. Zhang, L. Wang, Q. Lian, Y. Liu, J. He, D. Li, Z. Jin, Human lower extremity joint moment prediction: a wavelet neural network approach, Expert Syst. Appl. 41 (2014) 4422–4433.
[50] A. Subasi, A. Alkan, E. Koklukaya, M.K. Kiymik, Wavelet neural network classification of EEG signals by using AR model with MLE preprocessing, Neural Netw. 18 (2005) 985–997.
[51] A. Subasi, M. Yilmaz, H.R. Ozcalik, Classification of EMG signals using wavelet neural network, J. Neurosci. Methods 156 (2006) 360–367.
[52] R.A. Clayton, A.K. Amin, M.S. Gaston, I.J. Brenkel, Five-year results of the sigma total knee arthroplasty, Knee 13 (2006) 359–364.
[53] D.F. Dalury, R.A. Gonzales, M.J. Adams, T.A. Gruen, K. Trier, Midterm results with the PFC Sigma total knee arthroplasty system, J. Arthroplast. 23 (2008) 175–181.
[54] A.S. Ranawat, R. Rossi, I. Loreti, V.J. Rasquinha, J.A. Rodriguez, C.S. Ranawat, Comparison of the PFC Sigma fixed-bearing and rotating-platform total knee arthroplasty in the same patient: short-term results, J. Arthroplast. 19 (2004) 35–39.
[55] R. Willing, I.Y. Kim, Design optimization of a total knee replacement for improved constraint and flexion kinematics, J. Biomech. 44 (2011) 1014–1020.
[56] M. Ackermann, A.J. van den Bogert, Optimality principles for model-based prediction of human gait, J. Biomech. 43 (2010) 1055–1060.
[57] F.C. Anderson, M.G. Pandy, Dynamic optimization of human walking, Trans. Am. Soc. Mech. Eng. J. Biomech. Eng. 123 (2001) 381–390.

**Marzieh M. Ardestani** was born in Iran on August 1986. She received the B.S. degree in biomedical engineering and the M.S. degree in control engineering from the Isfahan University of Technology, Isfahan, Iran, in 2009 and 2011, respectively. She is currently working toward the Ph.D. degree in computational biomechanics at Xi'an Jiaotong University, Xi'an, China. Her academic interests are in the areas of Human movement, knee rehabilitation, and artificial intelligence.

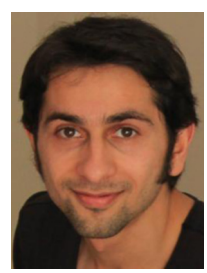

**Mehran Moazen** graduated in Mechanical Engineering from University of Mazandaran (Iran) in 2005 and completed his Ph.D. in Medical Engineering at the University of Hull (UK) in 2008. In 2009, he moved to University of Leeds (UK) as a Post-doctoral Research Fellow. He is currently working as Royal Academy of Engineering Research fellow at the University of Hull. His research interests are focused on the biomechanics of bone and joints, to understand the underlying mechanisms of growth, adaptation and repair.

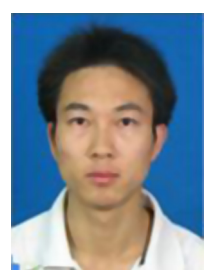

**Zhenxian Chen** was born in China on May 1986. He received the B.S. degree in mechanical engineering from Chengdu University of Technology; Chengdu, China in 2010. He got his M.S. degree from Xi'an Jiaotong University, Xi'an, China in 2012. He is currently working toward the Ph.D. degree in computational biomechanics at Xi'an Jiaotong University. His academic interests are in the areas of knee joint contact mechanics, human movement science, and musculoskeletal modeling.

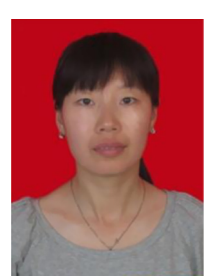

**Jing Zhang** was born in China on February 1986. She obtained Bachelor of Engineering Science from Harbin Engineering University, Harbin, China in 2009. She got master degree from Xi'an Jiaotong University, Xi'an, China in 2012. She is currently working toward the Ph. D. degree in Xi'an Jiaotong University. Her academic interests are in the areas of artificial knee joints contact mechanics, and UHMWPE wear mechanics.

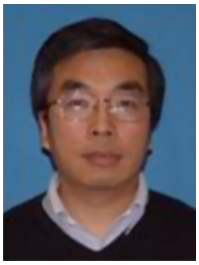

**Zhongmin Jin** is 'Thousand plan' honored professor in Xi'an Jiaotong University, Xi'an, China, spend the past two decades on the research of tribology of artificial joints, who had built the theoretical and computational modeling system in this field with great impact in the artificial joint prosthesis design. Prof. Jin is now a member of British Mechanical Engineering Institute, member of the Chinese mechanical engineering organization and tribology branch, with work supported by EPSRC, Yorkshire Forward, Royal Academic of Engineering, Royal Society, Chinese NSFC, and Chinese Government. He has led a European Union COST (533) on Bio tribology project, which involved 18 countries, 50 members.